Effective interatomic forces and atomic and electronic structure of liquid and amorphous metals

1991 J. Phys.: Condens. Matter 3 F23

(http://iopscience.iop.org/0953-8984/3/42/003)

J. Phys.: Condens. Matter 3 (1991) F23–F38. Printed in the UK

Effective interatomic forces and atomic and electronic structure of liquid and amorphous metals

J Hafner

Institut für Theoretische Physik, Technische Universität Wien, Wiedner Hauptstrasse 8–10, A-1040 Wien, Austria

Received 22 May 1991

Abstract. The state of the art in the calculation of interatomic forces in s, p- and d-bonded metals and alloys, and their application in the atomistic simulation of the structural and electronic properties of liquid and amorphous phases are reviewed.

1. Introduction

The theory of effective interatomic forces in condensed matter continues to be a subject of intense research effort [1, 2]. Accurate knowledge of interatomic interactions is especially important in investigations of liquid and amorphous materials, where only atomistic simulations based on quantum-mechanically derived interatomic forces can lead to a microscopic understanding of the atomic and electronic structures. For the s,p-bonded or simple metals pseudopotential perturbation theory has led to a thorough understanding of the variation of the interatomic potentials across the periodic table [3, 4], and of the relation of these changes to the trends in the crystalline [3] and liquid [5] structures and in the electronic spectra [6–8]. It is surprising how far this simple concept of competing pair and volume forces can be extended: even in liquid semiconductors such as *l*-As [9,10] or *l*-Te [11], qualitative differences between a second-order pseudopotential calculation and an *ab-initio* molecular-dynamics simulation based on quantum-mechanical many-body forces appear only at the level of four-body correlation functions. The consequences of this important result for the modelling of semi-empirical many-body forces are evident. Alloys of the alkali- and alkaline-earth metals with polyvalent metals continue to attract the interest of physicists and chemists because of their outstanding structural and electronic properties. The extension of low-order perturbation theory to these polyanionic phases goes to the very limits of applicability of the technique, but is still extremely useful [13–15].

If the pseudopotential theory of interatomic forces in s,p-bonded systems is by now a well-established technique, the theory of interatomic forces in the s,d-bonded transition metals is still in its infancy. Embedded-atom approaches [16] and techniques based on second-moment approximations [17, 18] to the electronic density of states have been quite successful for the metals of the Cu- and Ni-groups, but their extension to metals with a half-filled d-band and to transition-metal alloys has proved to be difficult. However, recently a certain breakthrough has been achieved through the reintroduction of an old concept: the bond-order [19–21]. The bond-order Θ_{ij} for

0953-8984/91/420F23+16$03.50

a pair of atoms (i, j) counts the difference in the number of electrons in bonding and antibonding states formed by orbitals centered at sites i and j. At least formally, a pair interaction for atoms (i, j) is given by the product of the transfer-integral with the bond-order (although many-atom effects are included in Θ_{ij}). Workable strategies for the calculation of bond-order potentials [22–24] have been developed by Pettifor and co-workers for crystalline and by Hausleitner and Hafner [25, 26] for liquid and amorphous tight-binding systems. The new bond-order potentials allow for the first time atomistic simulations of liquid and amorphous transition-metal systems using quantum-mechanically calculated interatomic forces.

2. Liquid s,p-bonded metals

2.1. Effective interatomic interactions and pseudopotentials

Within second-order perturbation theory, the total energy is given by the sum of a volume-energy and a pair-interaction term. Higher-order contributions introduce many-body forces. The basic ingredients in any calculation are the ionic pseudopotential and the local-field corrections to the Hartree dielectric function. The fact that many choices are possible for both the local field terms and the pseudopotential has sometimes led to the impression that the effective pair-forces derived from pseudopotential theory are ill-defined. However, this is not so. If only those local field factors are considered as acceptable which satisfy all the relevant sum rules of the electron gas, the choice is narrowed down to a few alternatives [3, 4]. The dielectric function of Ichimaru and Utsumi [27] is a very acceptable compromise between accuracy and computational convenience. A similar statement applies to the choice of an ionic pseudopotential. Following the seminal work of Phillips and Kleinman [28] based on an orthogonalized-plane-wave (OPW) expansion of the valence states, the optimization of the convergence of the perturbation series [29] was considered to be a natural criterion for the selection of a pseudopotential. Later on, when the interest shifted to non-perturbative total energy calculations, the important criteria were transferability of the pseudopotential and plane-wave convergence, at the expense of the convergence of the perturbation series [30–32]. Very recently we have been able to show that the pseudopotential approach is flexible enough to allow for an optimization of the perturbation series, without compromising transferability and plane-wave convergence [33].

Figure1 shows the effective pair interaction for liquid As, calculated using the optimized OPW- and norm-conserving pseudopotentials (both nonlocal) and the simple local empty-core pseudopotential used in our analysis of the trends in interatomic potentials through the Periodic Table [3, 9, 11]. We find that from very different starting points we arrive at a well-converged result for the effective interatomic interactions.

2.2. Atomic structure

In our investigations of the liquid s,p-bonded elements we have shown that (i) the increasing distortion of the structure factors and pair correlation functions in the divalent elements from Mg to Hg, (ii) the occurrence of a rather unique, loosely packed structure in liquid Ga, but then the return to more close-packed structures in In and Tl, (iii) the complex open structures of liquid Si and Ge and the transition

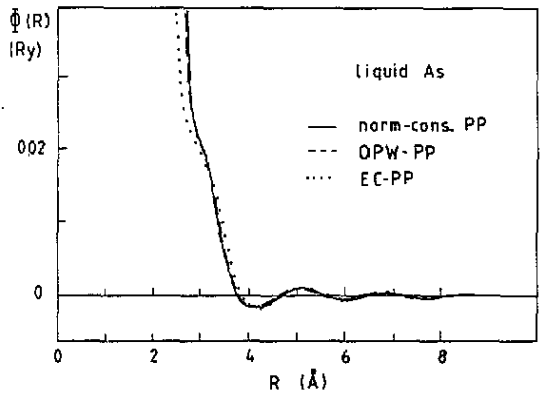

Figure 1. Effective pair forces for liquid arsenic calculated using an optimized norm-conserving pseudopotential (full curve), an optimized orthogonalized plane-wave pseudopotential (dashed curve), and using a local empty-core potential (dotted curve).

to close packed structures in Sn and Pb [6], (iv) the open structure of liquid As [9] with a short-range order that resembles closely to the crystalline structure (and similar anomalies in the structures of liquid Sb and Bi), and (v) even the chain-like structures of liquid Se and Te [11] arise from the modulation of the basic dense-random-packing structures by the Friedel oscillations in the effective interatomic interactions and the damping of these oscillations in the heavy elements. It is important to relate the pair-potential picture to the tight-binding arguments that are conventionally used to explain the structures of the semi-metallic and semiconducting elements of groups IV to VI.

2.2.1. Peierls distortion and Friedel oscillations. The classical explanation for the occurrence of three-fold coordination in the group V elements is based on a Peierls distortion of the structure. The electronic configuration of the free atom is s^2p^3. With a low-lying, non-bonding s-band only the p-electrons contribute to the formation of the chemical bond. With the six lobes of the p-orbitals forming right angles, this would lead to a sixfold-coordinated simple cubic structure. However, as the p-band is exactly half-filled, it is unstable against a Peierls-distortion leading to a dimerization of the bonds and threefold coordination. Similarly, for the group VI elements where the p-band is filled to two-thirds, a Peierls distortion leads to trimerization and the formation of chain-like structures. The most important factor for the occurrence of a Peierls distortion is the modulus of the on-Fermi-surface matrix element $|\omega(2k_F)|$ of the pseudopotential. It must be sufficiently large to stabilize the Peierls distortion against the restoring repulsive interatomic forces. The amplitude of the Friedel oscillations is proportional to $|\omega(2k_F)|^2$. The electron-per-atom ratio determines the position of the nearest-neighbour distance relative to the minima and maxima of the Friedel oscillations (in the same way as it determines the band-filling in a reciprocal space picture). This is illustrated in figure 2 for Al, Ge, As and Te. In Al, the nearest neighbour distance in a close-packed, hard-sphere-like fluid falls right into the first minimum of the potential. In Ge, As, and Te the close-packing distance falls on a repulsive hump of the pair interaction. Evidently in such a case it is energetically favourable to split the nearest neighbour shell such as to move the atoms into the adjacent minimas or inflections of the potential at $R_1 \simeq D_{cp} - l_F/2$ and $R_2 \simeq D_{cp} + l_F/2$ where D_{cp} is the close-packing distance and $l_F = 2\pi/2k_F$ the

wavelength of the Friedel oscillations. Thus we find that the pair potential argument is just the appropriate real-space formulation of a Peierls instability.

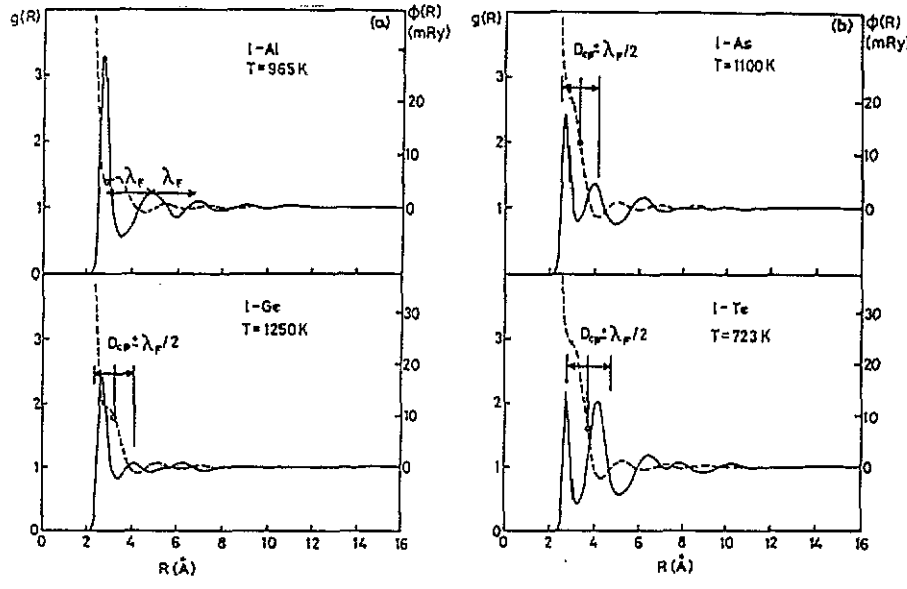

Figure 2. Interatomic potentials $\phi(R)$ and pair correlation functions g(R) for liquid Al, Ge, As and Te. The open circles mark the nearest-neighbour distance D_{cp} for close-packing. The 'Peierls-distortion' occurring in Ge, As, and Te is indicated (cf. text)

At the level of a pair correlation function there are hardly any detectable differences between the result of a molecular-dynamics simulation based on pseudopotential-derived pair forces, even for semiconducting liquids such as As and Te. The limitations of the simple perturbation theory appear only in a comparison with the three- and four-body correlation functions from *ab-initio* density functional molecular dynamics. Even at the level of three-body correlation functions (bond-angle distributions), there are but small quantitative differences in liquid Si, As, and Se [9–11, 34]. Qualitative differences appear only at the level of four-body correlations (distribution of the average heights of trigonal pyramids in *l*-As, distribution of the dihedral angles in *l*-Se and *l*-Te), see figure 3. However, these four-body correlations turn out to be very important for the formation of an energy gap at the Fermi surface in *l*-As and in *l*-Se and Te (see below).

2.2.2. Empirical many-body forces. There have been many attempts to construct many-body forces for atomistic simulations of semiconductors [35–37]. It is quite astonishing that these attempts deliberately ignore the messages of pseudopotential theory: the volume term is omitted and the leading pair potential term gives a close-packed atomic arrangement. Hence it is not surprising that strong three-body forces are necessary to reduce the coordination number from $N_c \approx 10$–12 to $N_c \approx$ 6–7 in *l*-Si. However, these strong angular forces lead to bond-angle distributions in bad agreement with *ab-initio* simulations. If three-body forces are added to the pseudopotential-derived pair- and volume-forces, one finds that only very weak three-body forces are necessary to match the result of the *ab-initio* simulations for the

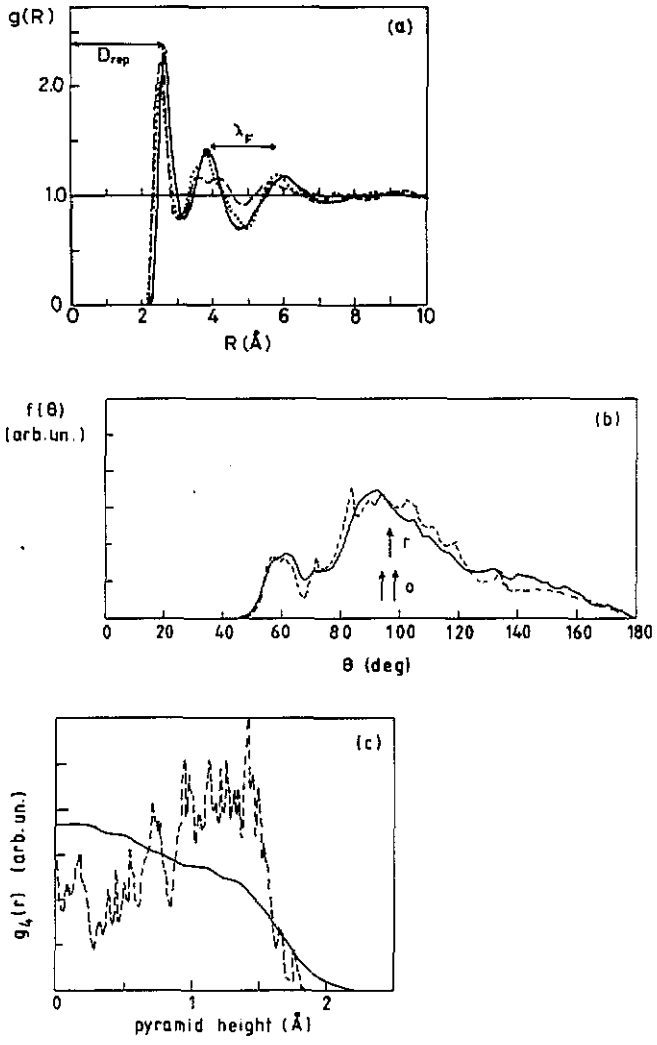

Figure 3. Pair- and many-body correlation functions in liquid As: (*a*) pair correlation function $g(R)$, (*b*) bond-angle-distribution function, and (*c*) distribution of the average height of trigonal As_4 pyramids. Dashed curve: density functional molecular dynamics [10], full curve: molecular dynamics using pair potentials from a pseudopotential perturbation expansion [9], circles: experiment.

liquid, but relatively strong three-body forces are necessary to stabilize the transverse acoustic phonons of the crystal [38]. Thus we arrive at the not unexpected conclusion that many-body forces are strongly state dependent.

2.3. Electronic spectra

The fact that accurate atomistic simulations are now available for all simple liquid metals has enabled us to perform self-consistent calculations of the electronic structure using a supercell method based on linearized muffin-tin orbitals (LMTOs) [6–8] and using a dynamical simulated annealing (DSA) approach [39]. The results shown in figure 4 display several interesting features:

(i) For the first row elements Li and Be we find a strong reduction of the width of the occupied band and pronounced structure-induced minima in the electronic density of states (DOS).

(ii) The second row elements from Na to Si are the only ones with an almost free-electron DOS.

(iii) s–d hybridization and the relativistic lowering of the d-states relative to the s-states induce a deviation from a free-electron DOS in the heavy alkali and alkaline earth metals. Liquid Ba is found to be a transition metal with about 0.74 d-electrons per atom.

(iv) In the IIb elements Zn, Cd, and Hg theory predicts a progressive lowering of the DOS at the Fermi level, in agreement with the Mott model for liquid mercury.

(v) In the heavy polyvalent metals In, Tl, Ge, Sn, Pb, Sb, and Bi we predict deep pseudogaps, resp. gaps separating s- and p-bands. The appearance of a gap in the valence-band is directly related to the damping of the oscillations in the interatomic potentials and to the return to close-packed structures [6]. In the heavier elements the position q_0 of the first zero in the pseudopotential form factor moves toward $q = 2k_F$ and this leads on one hand to an increase of the matrix element for $q = Q_p$ (where Q_p is the position of the main peak in the structure factor), and hence to a broadening of the structure-induced gap at an energy of $(\hbar^2 Q_p^2/2m)$ above the bottom of the band, and on the other hand to a decrease of the $q = 2k_F$ matrix element and a damping of the Friedel oscillations.

(vi) The predictions are in quantitative agreement with the most recent results of photoelectron spectroscopy for the liquid metals [40, 41]. A detailed comparison requires the calculation of the partial photoionization cross-sections as a function of the binding energy of the photoelectron and of the energy of the exciting photon [6, 7, 42].

(vii) In the liquid semiconductors the correct description of the four-body correlations turns out to be essential for the formation of a gap at the Fermi level [10, 34, 39].

3. Liquid s,p-bonded alloys

Binary alloys of the s,p-bonded metals with a sufficiently large difference in the valence of the components form compounds with widely different bonding properties: salt-like compounds, polyanionic cluster compounds, and intermetallic phases [43]. Salt-like bonding and polyanionic clustering persists even in the liquid state [44]. The formation of the polyanionic phases obeys a generalized Zintl principle: the atomic arrangement in the anionic complexes corresponds to the structure of the element having the same number of valence electrons [45]. It has been shown that the occurrence of salt-like chemical order [46] and of polyanionic clustering [14, 15] in alloys of the alkali metals with group-IV elements can be reasonably well explained within the framework of pseudopotential theory. Changes in the screening and in the pseudopotentials lead to strong anion-cation and anion-anion forces, and whether this leads to salt-like-ordering or polyanionic clustering is determined largely by the anion/cation size ratio. Here I want to address the formation of extended anionic sublattices and their equivalent in the liquid phase. The classical example is provided by the NaTl-type Zintl phases in the I–III alloys: assuming complete electron transfer, the group-III element acquires the electronic configuration of a group-IV element and forms a diamond-type sublattice stabilized by strong sp^3-bonds [47, 48]. This picture

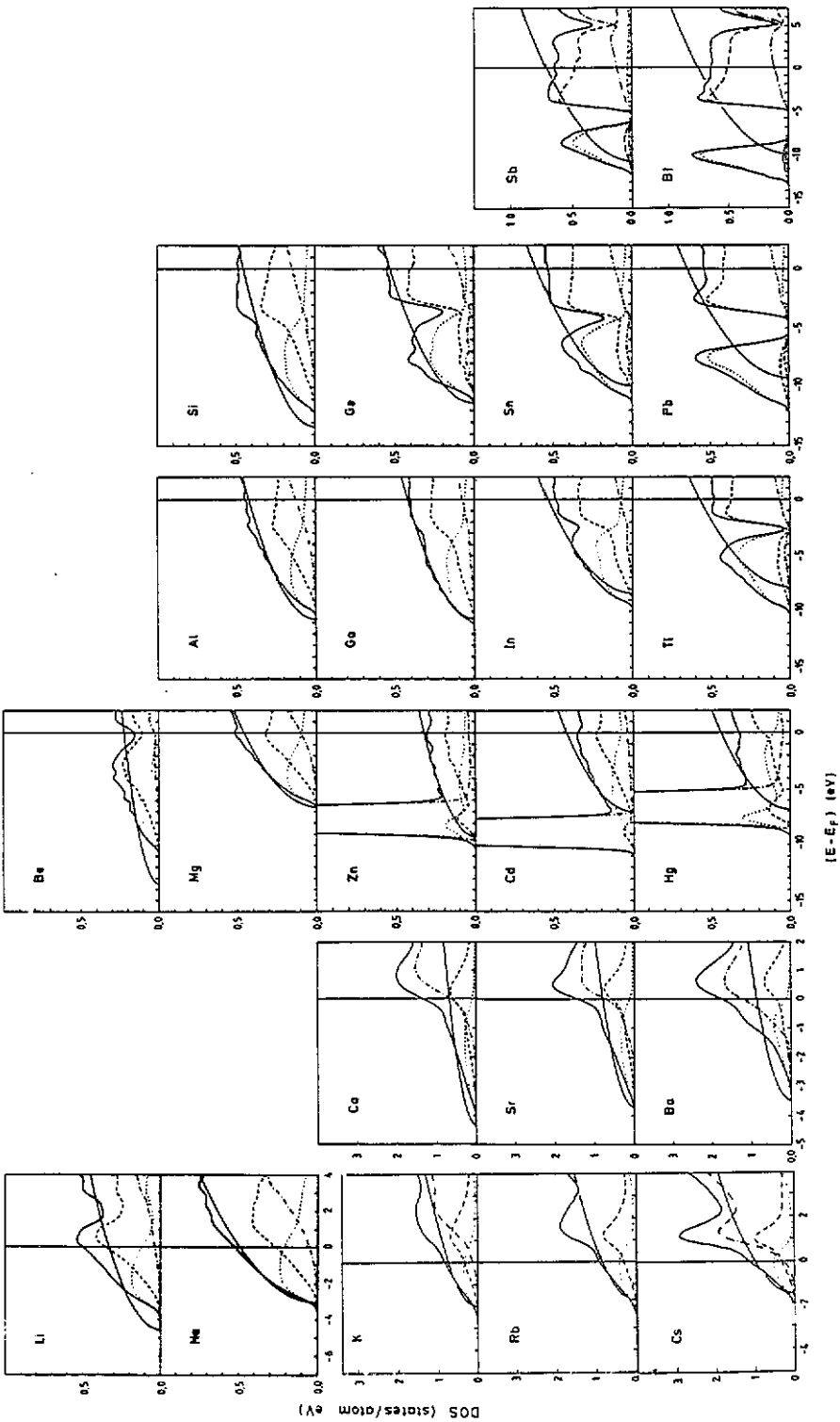

Figure 4. Electronic density of states for the liquid s,p-bonded metals. Full curve: total DOS, dotted curve: s-electron contribution, dashed curve: p-electron contribution, dot dashed curve: d-electron contribution. The free-electron parabola is shown for comparison.

has even more general validity. In the Li–Ga and Li–Al systems, As-type Ga(Al)-sublattices are found in the crystalline compounds Li_3Ga_2 (Li_3Al_2), and chains of Ga (Al) atoms like in Se are formed in Li_2Ga and in Li_9Al_4 (see [49]). Neutron diffraction experiments point to a persistence of a short-range order into the liquid state [50]. The changes in the interatomic interactions on alloying are dominated by the reduced screening of the polyvalent ions. This leads to an increase of the oscillations in the Ga–Ga potential and to a strong Li–Ga interaction (figure 5). The molecular dynamics simulations [13] show that this results in Ga–Ga correlations in the liquid alloys that are distinctly Ge-, As-, and Se-like with increasing Li-content of the alloy (figure 6). At a composition of 70 to 80% Li, we find broken, entangled Ga-chains immersed in a Li-matrix—in striking analogy to the structure of molten Se and Te (figure 7). The investigations of the electronic spectra supports the validity of the generalized Zintl principle: Liquid $Li_{50}Ga_{50}$ has an electronic DOS that resembles closely that of molten Ge. The destruction of strong angular correlation on melting leads to a breakdown of sp^3-hybridization and the formation of well-separated s- and p-bands. This type of electronic DOS persists at higher Li-content. It shows that the strong Ga–Ga bonds predicted by the interatomic interactions are of a ($pp\sigma$)-type. Of course the description of polyanionic clustering goes again to the very limits of applicability of such a simple theory. First attempts have been made to apply *ab-initio* molecular dynamics to this problem [51]. The results confirm the conclusions drawn from the simple perturbation calculations.

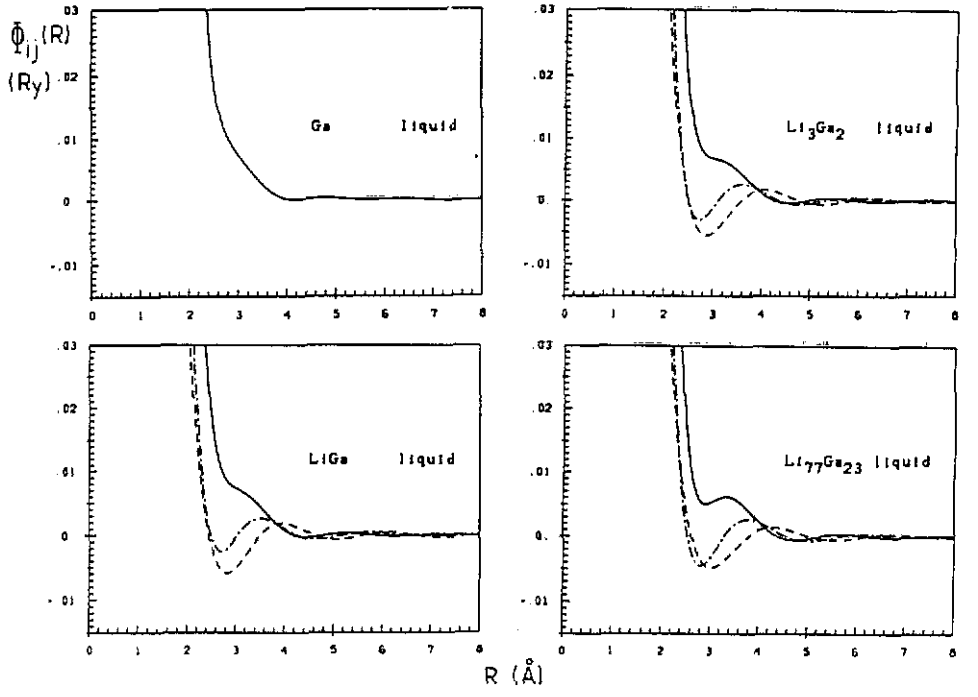

Figure 5. Effective pair interactions in Li–Ga alloys. Full curve: Ga–Ga, dashed curve: Li–Li, dot dashed curve: Li–Ga.

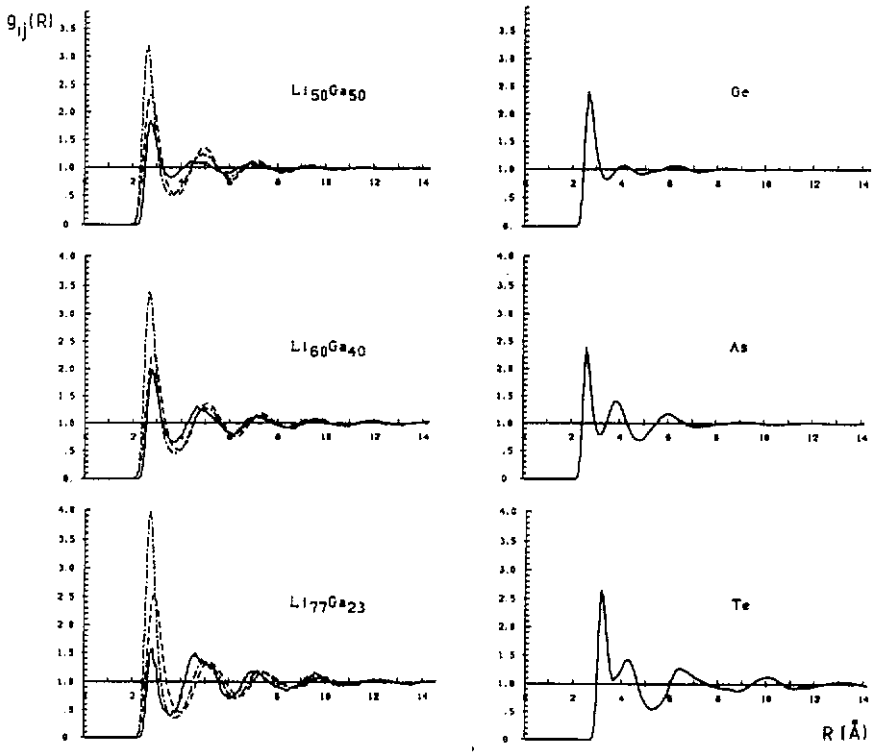

Figure 6. Partial pair correlation functions in liquid Li–Ga alloys calculated by molecular dynamics. Full curve: Ga–Ga, dashed curve: Li–Li, dot dashed curve: Li–Ga. the comparison of the Ga–Ga correlation functions with those of liquid Ge, As and Te demonstrates the validity of an extended Zintl principle (see text).

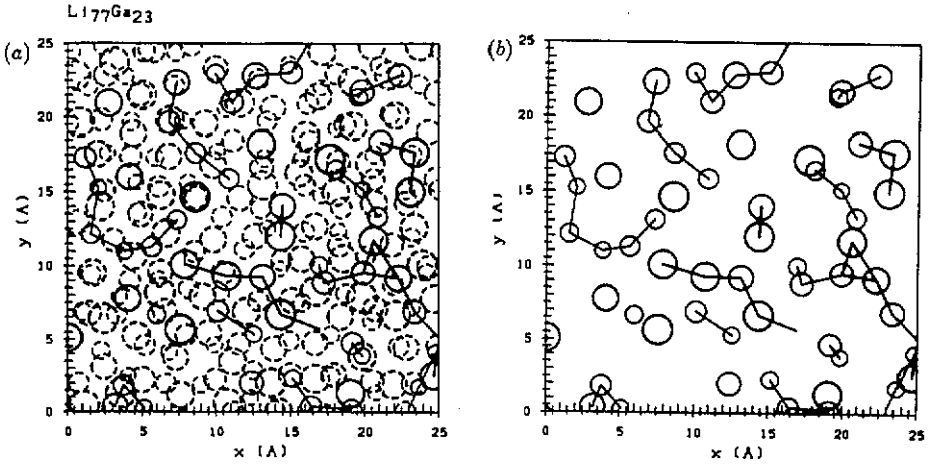

Figure 7. An instantaneous configuration of liquid $Li_{77}Ga_{23}$. Broken circles: Li atoms, full circles: Ga atoms. Nearest-neighbour Ga–Ga bonds are drawn. The size of the symbols is scaled with the z-coordinate. Part (b) repeats the same configuration with the Li atoms omitted for the sake of clarity.

4. Liquid transition metals

The correct description of the properties of liquid transition metals have been a long-standing challenge to condensed matter theorists. Recently we have succeeded in developing realistic interatomic forces for s–d bonded metals and alloys [25, 26]. The basic assumption is that the total energy may be decomposed into contributions from s- and d-electrons. The s-electron part is treated using conventional pseudopotential theory. The d-electron energy may be written within a tight-binding-bond (TBB) approximation as the sum of a repulsive term and a bonding term, $E_d = E_{d,rep} + E_{d,bond}$. The repulsive term may be parametrized in terms of a pair interaction provided by the electrostatic, exchange-correlation and non-orthogonality contributions to the total energy [17, 21]. $E_{d,bond}$ measures the covalent bond energy resulting from the formation of a d-band with the density of states $n(E)$. Quite generally the covalent bond energy may be written as [21–23]

$$E_{d,\,bond} = \frac{1}{2}\sum_{\substack{i,j \\ i\neq j}} h_{ij}(R_{ij})\,\Theta_{ij} \tag{1}$$

where $h_{ij}(R_{ij})$ is the transfer integral and Θ_{ij} is the bond-order which is defined as the difference between the number of electrons in the bonding $\varphi_+ = 1/\sqrt{2}(\varphi_i - \varphi_j)$ and in the antibonding states $\varphi_- = 1/\sqrt{2}(\varphi_i - \varphi_j)$ (the indices i and j stand for the atomic site as well as the orbital). It may be shown that the bond-order may be expressed in terms of the difference between the bonding and antibonding Greens functions $G_\pm(E) = \langle\varphi \pm |(H-E)^{-1}|\varphi\pm\rangle$ or in terms of the off-diagonal Greens function $G_{ij}(E) = \langle\varphi_i|(H-E)^{-1}|\varphi_j\rangle$. Assuming all five orbitals to be degenerate, these Greens functions may be calculated analytically on a Bethe-lattice reference system [25, 26]. For a pure metal, the result is equivalent to a second-moment approximation to the DOS in the limit of high coordination numbers [17]. For an alloy, the bond order varies strongly with the form of the d-band and the band-filling. Note that in the Bethe-lattice approximation the state- and configuration-dependence of the bond order enters only via the coordination number and the chemical short-range order, and (1) reduces to a sum over pair-interactions.

A typical transition metal pair potential is shown in figure 8. Around the nearest-neighbour distance it is composed of strong attractive d-interactions and repulsive s-electron interactions. TM-interactions have rather unique features: (i) extreme softness (at thermal energies above the minimum of the potential, the slope of $\phi(R)$ is distinctly smaller than for s,p-bonded metals) and (ii) strong attractive minimum (measured in units of $k_B T_M$, the potential minimum is up to five times stronger than in simple metals, T_M is the melting temperature). Due to the combination of these features, liquid TM are rather a challenge to liquid state theory. In fact, all current techniques fail except for TM with a nearly full band (Ni,Pd) [52]. Molecular dynamics simulations yield good agreement with diffraction data for all 4d-metals and the 3d-metals except Sc and Ti (figure 8) and provide the basis for the first selfconsistent calculation of the electronic structure of molten TM [53].

5. Liquid and amorphous transition metal alloys

The amorphous TM alloys produced by quenching from the liquid state have received much attention. Neutron diffraction studies [54] have demonstrated that these alloys

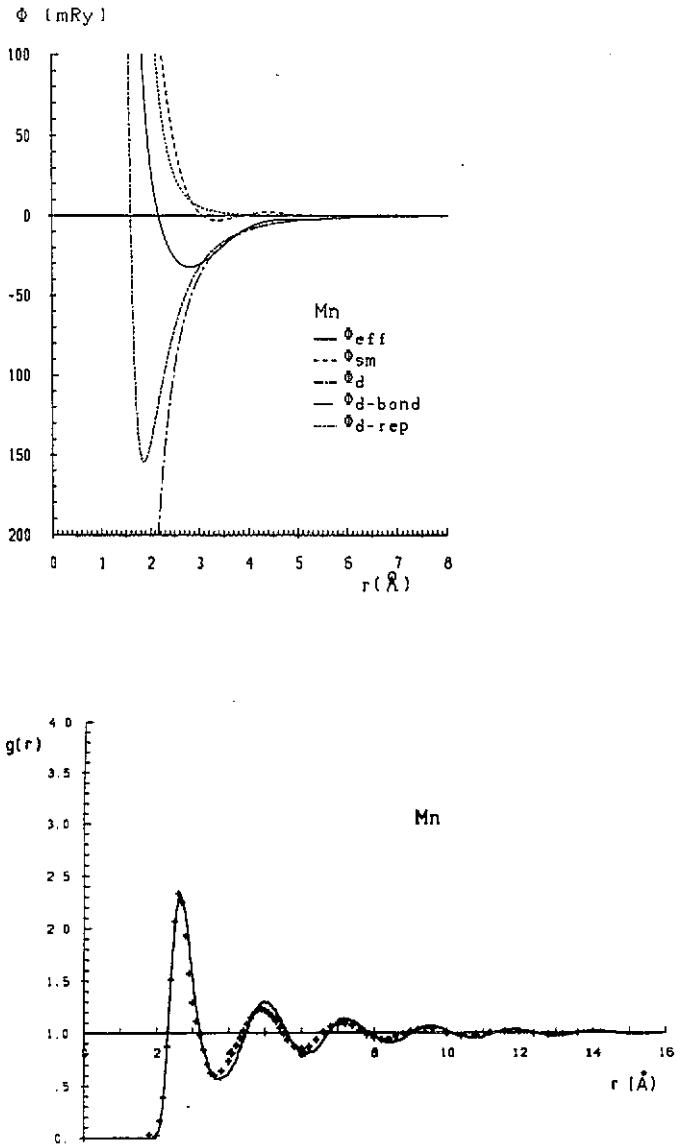

Figure 8. (*a*) Effective pair-interaction $\phi(R)$ and (*b*) pair-correlation $g(R)$ for liquid Mn (crosses: diffraction data).

have a high degree of chemical as well as topological order, photoemission studies revealed strong electronic bonding effects that are incompatible with any simple rigid or common-band model [55, 56]. It turns out that the TBB-forces are sufficiently realistic to describe the structural and electronic properties of amorphous TM alloys. At a large difference in the atomic d-electron eigenvalues (or equivalently for a large difference in the group number) of the components, e.g. in Ni–Y, the alloy is close to the split-band limit. The lower part of the band is a nearly full Ni-

band, the upper part a Y-band (figure 9). Consequently, bonding and antibonding contributions compensate each other nearly completely in Ni–Ni-bonds, while only bonding contributions are counted for the Y–Y and Ni–Y bond orders. This leads to strongly non-additive pair forces (figure 10) with a strong preference for the formation of Ni–Y pairs and very short Ni–Y bond distances. The non-additivity disappears gradually as Y is substituted by a metal with more d-electrons [25, 26].

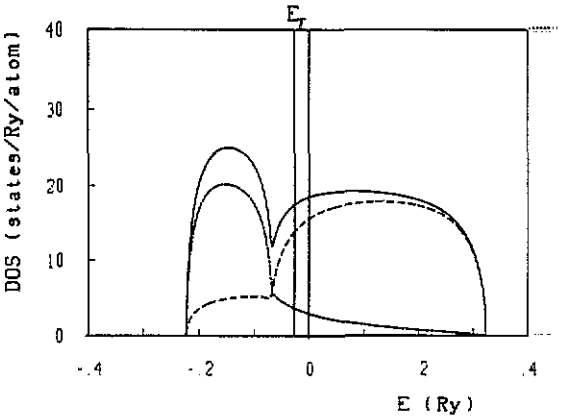

Figure 9. Total and partial electronic density of states for a $Ni_{33}Y_{67}$ alloy calculated on a Bethe lattice.

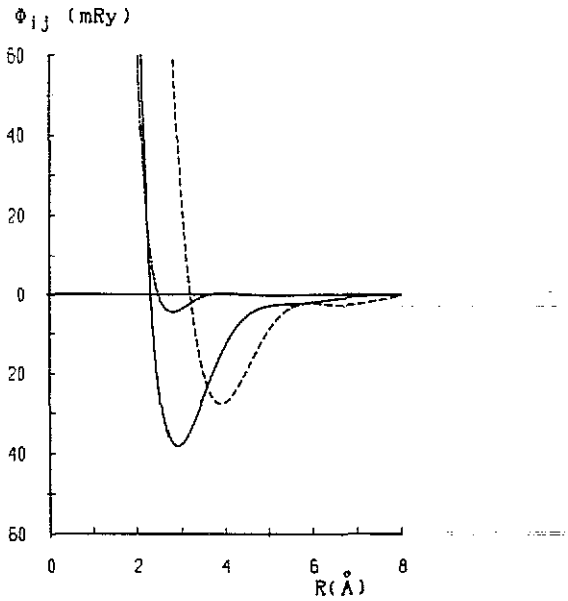

Figure 10. Effective pair interactions for a disordered Ni–Y alloy calculated using the hybridized nearly-free-electron tight-binding-bond approach.

A molecular dynamics simulation (equilibration in the liquid phase, fast cooling at a rate of $\dot{T} \simeq 10^{12}$ K s^{-1}, low-temperature annealing) yields a structure of the

glassy phase in good agreement with experiment for all Ni-based glasses for which partial correlation functions have been measured. For amorphous $Ni_{50}Zr_{50}$ we find a high degree of chemical short-range order and a topological short-range order that is astonishingly similar to the crystalline NiZr (CrB-type) compound (figure 11). The strong ordering effects are directly related to the non-additivity of the pair forces. A detailed analysis shows that in Ni–Y, Zr, Ti alloys the short-range order is of a trigonal-prismatic type, in Ni–Nb glasses the local order changes to a weaker chemical order and a polytetrahedral local topology [25,26]. Calculated and measured photoemission intensities [57] for amorphous Ni–Zr alloys and the crystalline compound $NiZr_2$ ($CuAl_2$-type) are given in figure 12. This result is important not only because of the good agreement between theory and experiment, but also because it shows that the Bethe-lattice calculation gives a rather realistic description of the electronic structure of the amorphous alloys. This shows that interatomic forces, atomic and electronic structure are reasonably consistent.

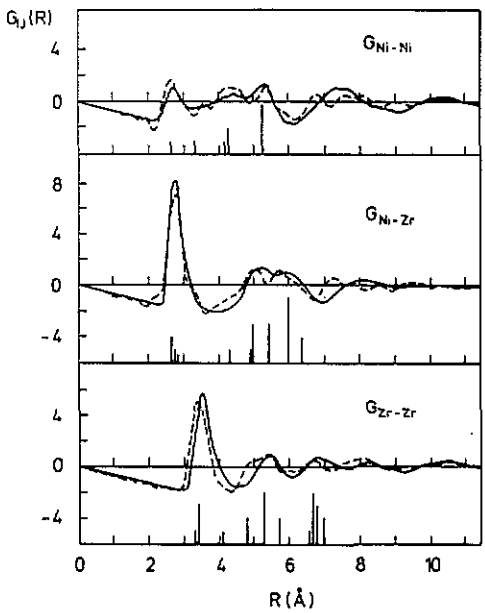

Figure 11. Partial pair correlation functions in amorphous $Ni_{50}Zr_{50}$. Full curve: MD simulation, dashed curve: experiment. The vertical bars indicate the nearest-neighbour distances in the crystalline NiZr compound.

6. Conclusions

I have attempted to give an overview of the state of the art in the calculation of effective interatomic forces in metallic systems. For the simple metal systems, pseudopotential-derived interatomic forces have enabled us to interpret all the interesting trends in the atomic and the electronic structure in the molten phase. These techniques also make interesting contributions to the investigation of salt-like and polyanionic liquid alloys. For the transition-metal systems, the use of a hybridized nearly-free-electron–tight-binding technique and the introduction of the concept of

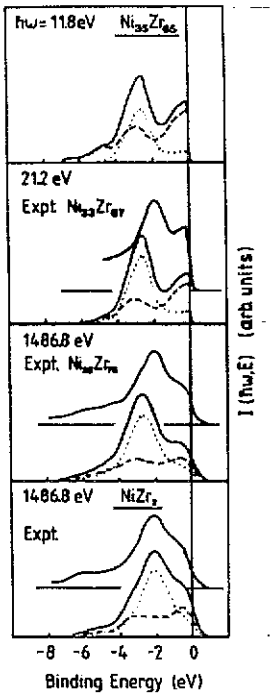

Figure 12. Calculated and measured photoemission intensities for Ni–Zr glasses and the crystalline compound $NiZr_2$. The dotted and dashed curves in the calculated spectra show the Ni- and Zr-contributions to the emitted photoelectron intensity.

the bond-order has led to an important step forward. We can now calculate accurate interatomic forces for transition metals and their alloys using techniques that are essentially rigorous and derived from first principles. The challenge is now to achieve a similar result for the p–d systems (transition metal–metalloid, transition metal–aluminium etc).

Acknowledgments

It is a pleasure to acknowledge the important contributions of C Hausleitner, W Jank, and G Kahl to the work described in this paper. This research has been supported by the Fonds zur Förderung der wissenschaftlichen Forschung and by the Bundesministerium für Wissenschaft und Forschung.

Note added in proof. Very recently, the investigations of the amorphous TM alloys have been extended to $(Fe, Co, Ni)_xZr_{1-x}$ alloys. We have demonstrated that self-consistent spin-polarized electronic structure calculations predict the magnetic phase diagram with high accuracy and provide a convincing explanation for the non-collinear spin structures observed in the Fe-rich Fe_xZr_{1-x} glasses [58].

References

[1] Nieminen R M, Puska M J and Manninen M (ed) 1990 *Many-Atom Interactions in Solids* (Berlin: Springer)

[2] Vitek V (ed) 1989 *Atomistic Simulation of Materials beyond Pair Potentials* (New York: Plenum)
[3] Hafner J and Heine V 1983 *J. Phys. F: Met. Phys.* **13** 2479
[4] Hafner J 1987 *From Hamiltonians to Phase Diagrams* (Berlin: Springer)
[5] Hafner J and Kahl G 1984 *J. Phys. F: Met. Phys.* **14** 2259
[6] Jank W and Hafner J 1990 *Phys. Rev.* B **41** 1497; *Phys. Rev.* B **42** 6926, 11530
[7] Jank W and Hafner J 1990 *J. Phys.: Condens. Matter* **2** 5065
[8] Hafner J and Jank W 1990 *J. Phys.: Condens. Matter* **2** SA239
[9] Hafner J 1989 *Phys. Rev. Lett.* **62** 784
[10] Li X P, Allen P B, Car R, Parrinello M, and Broughton JQ 1990 *Phys. Rev.* B **41** 3260
[11] Hafner J 1990 *J. Phys.: Condens. Matter* **2** 1271
[12] van der Lugt W 1991 *Proc. Conf. on Physics of Fluids (Oxford, 1991)* (Bristol: Institute of Physics) at press
[13] Hafner J and Jank W 1991 *Phys. Rev.* B **44** at press
[14] Hafner J 1989 *J. Phys.: Condens. Matter* **1** 1133
[15] Hafner J 1990 *J. Non-Cryst. Solids* **117+118** 64
[16] Daw M S 1990 *Many-Atom Interactions in Solids* ed R M Nieminen, M J Puska and M Manninen (Berlin: Springer) p 48
[17] Wills J H and Harrison W A 1983 *Phys. Rev.* B **28** 4363
[18] Finnis M W and Sinclair J E 1984 *Phil.Mag.* A **40** 45
[19] Coulson C A 1939 *Proc. R. Soc.* A **169** 413
[20] Abell G C 1985 *Phys. Rev.* B **31** 6184
[21] Sutton A P, Finnis M W, Pettifor D G, and Ohta Y 1988 *J. Phys. C: Solid State Phys.* **21** 35
[22] Pettifor D G 1990 *Many-Atom Interactions in Solids* ed R M Nieminen, M J Puska and M Manninen (Berlin: Springer) p 64
[23] Pettifor D G 1989 *Phys. Rev. Lett.* **63** 2480
[24] Pettifor D G and Aoki H 1991 *Phil. Trans. R. Soc.* A **334** 439
[25] Hausleitner C and Hafner J 1990 *J. Phys.: Condens. Matter* **2** 6651
[26] Hausleitner C and Hafner J 1990 *Phys. Rev.* B **42** 5863; 1991 *Phys. Rev.* B **44** at press
[27] Ichimaru S and Utsumi K 1981 *Phys. Rev.* B **24** 7385
[28] Phillips J C and Kleinman L 1959 *Phys. Rev.* **116** 287
[29] Cohen M H and Heine V 1961 *Phys. Rev.* **122** 1821
[30] Bachelet G B, Hamann D R, and Schlüter M 1982 *Phys. Rev.* B **26** 4199
[31] Vanderbilt D 1985 *Phys. Rev.* B **26** 4199
[32] Rappe A, Rabe K, Kaxiras E and Joannopoulos J D 1990 *Phys. Rev.* B **41** 1227
[33] Kresse G, Hafner J and Needs R 1991 unpublished
[34] Hohl D and Jones R O 1990 *J. Non-cryst.Solids* **117+118** 922
[35] Stillinger P R and Weber T A 1985 *Phys. Rev.* B **31** 5262
[36] Biswas R and Hamann D R 1985 *Phys. Rev. Lett.* **55** 2001
[37] Tersoff J 1986 *Phys. Rev. Lett.* **56** 632
[38] Mauser N and Hafner J 1991 unpublished
[39] Hafner J and Payne M C 1990 *J. Phys.: Condens. Matter* **2** 221
[40] Indlekofer G, Oelhafen P, Lapka R and Güntherodt H J 1988 *Z.Phys.Chem.* **157** 465
[41] Indlekofer G and Oelhafen P 1990 *J.Non-Cryst.Solids* **117+118** 340
[42] Redinger J, Marksteiner P and Weinberger P 1986 *Z. Phys.* B **63** 321
[43] Zintl E and Kaiser H 1933 *Z. Anorgan. Allg. Chem.* **211** 113
[44] van der Lugt W and Geertsma W 1987 *Can.J.Phys.* **65** 326
[45] Klemm W and Bussmann E 1963 *Z. Anorg. Allgem. Chem.* **319** 297
[46] Pasturel A, Hafner J and Hicter P 1985 *Phys. Rev.* B **32** 5009
[47] Christensen N E 1985 *Phys. Rev.* B **32** 207
[48] Hafner J and Weber W 1985 *Phys. Rev.* B **33** 747
[49] Müller W and Stöhr J 1977 *Z. Naturf.* **32 b** 631
[50] Reijers H T J, van der Lugt W, van Tricht J B, Vlak W A and Howells W S 1989 *J. Phys.: Condens. Matter* **1** 8609
[51] Galli G and Parrinello M 1990 *J. Phys.: Condens. Matter* **2** SA227
[52] Hausleitner C, Kahl G and Hafner J 1991 *J. Phys.: Condens. Matter* **3** 1589
[53] Jank W, Hausleitner C and Hafner J 1991 *J. Phys.: Condens. Matter* submitted
[54] Suzuki K 1990 *J. Non-Cryst. Solids* **1** 117–118
[55] Oelhafen P 1983 *Glassy Metals* II ed H Beck and H J Güntherodt (Berlin: Springer) p 284

[56] Oelhafen P 1987 *Liquid and Amorphous Materials* ed E Lüscher, G Fritsch and G Jacucci (Dordrecht: Martinus Nijhoff) p 333
[57] Jank W and Hafner J 1991 *Europhys. Lett.* at press
[58] Hafner J, Hausleitner C, Jank W and Turek I 1991 *Proc. 5th Int. Conf. on the Structure of Non-crystalline Materials (NCM5), J. Non-cryst. Sol.* at press